Journal of Power Sources 246 (2014) 719–728

Contents lists available at ScienceDirect

Journal of Power Sources

journal homepage: www.elsevier.com/locate/jpowsour

Evaluation of performance and operation viability of non-uniform potential solid oxide fuel cell fueled by reformed methane

P. Piroonlerkgul [a], W. Kiatkittipong [b], S. Wongsakulphasatch [b], F. Aiouache [c], S. Assabumrungrat [a,*]

[a] Center of Excellence in Catalysis and Catalytic Reaction Engineering, Department of Chemical Engineering, Faculty of Engineering, Chulalongkorn University, Bangkok 10330, Thailand
[b] Department of Chemical Engineering, Faculty of Engineering and Industrial Technology, Silpakorn University, Nakhon Pathom 73000, Thailand
[c] Department of Engineering, Faculty of Science and Technology, Lancaster University, Lancaster LA1 4YR, United Kingdom

HIGHLIGHTS

- The performance of SOFC with non-uniform potential operation was evaluated.
- Maximum stack temperature gradient and stack temperature were considered.
- Non-uniform potential SOFC stacks with a cooler show higher performance.

GRAPHICAL ABSTRACT

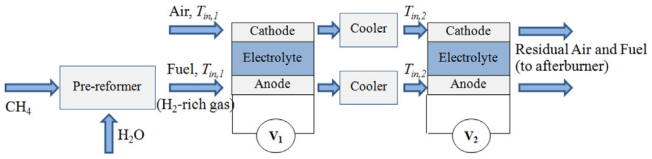

ARTICLE INFO

Article history:
Received 11 June 2013
Received in revised form
16 July 2013
Accepted 31 July 2013
Available online 15 August 2013

Keywords:
Solid oxide fuel cell
Non-uniform potential
Methane
Operation viability
Two-stacks

ABSTRACT

The performance and the operation viability of solid oxide fuel cells (SOFC) fueled by reformed methane using the concept of non-uniform potential operation were evaluated by one-dimensional finite difference analysis. Two thermal constraints including maximum acceptable stack temperature gradient and maximum stack temperature were the criteria for considering the operation viability. The average power density was used as a performance indicator. In addition, two major process parameters: fuel and air inlet temperatures and the operating voltage were examined to determine the suitable values for different viabilities. The results revealed that non-uniform potential SOFC with two stack sections operating at different voltages could not offer a significantly higher average power density compared with the uniform potential SOFC owing to thermal constraint limitations. The installation of coolers between the stacks is important and it could offer 12.8% improvement in average power density.

1. Introduction

Due to the continuous increase in fossil fuel price, alternative developments of high-performance and environmental-friendly technologies for electricity generation are desirable. Fuel cell technologies have been of interest over the last decade owing to higher electrical efficiency compared with conventional combustion heat engines [1]. This is due to the direct conversion of chemical energy to electrical energy via electrochemical reactions whilst a prior conversion of the chemical energy to thermal and mechanical energies takes place in the combustion heat engines along with greater irreversible losses. Among various types of fuel cells, the solid oxide fuel cell (SOFC) is a promising technology as it offers number of advantages: (1) high operating temperature which enhances the rate of electrochemical reactions and inhibits the overpotential losses, (2) improved electrical efficiency as the high-temperature exhaust gas (1073–1273 K) is utilized to produce additional electricity via gas turbine/engine cycle [1,2], and (3) fuel sources such as methane, ethanol, natural gas or oil derivatives can be used without pre-processing constraints.

* Corresponding author.
E-mail address: Suttichai.A@chula.ac.th (S. Assabumrungrat).

0378-7753/$ – see front matter © 2013 Elsevier B.V. All rights reserved.
http://dx.doi.org/10.1016/j.jpowsour.2013.07.120

The improvement of SOFC performance has been performed using three main methods: the development of a new component material to offer a low overpotential loss [3,4], the combination of SOFC stack with heat engines to generate additional electricity [5,6] and the optimization of operating conditions [7]. Among the optimization techniques, concept of using the so-called "non-uniform potential operation" is of interest [8–11]. In this concept, a SOFC stack is divided into several sections and operated at different operating voltages. Near the entrance of the fuel cell stack, where H_2 concentration in fuel gas and rate of electrochemical reaction are high, a high value of cell voltage is used to maximize the power density. Inversely, near the exit of the stack, low cell voltage is set to maintain SOFC power density at a high value although the electrochemical reaction rate is low due to low H_2 concentration of the fuel gas. Selimovic and Plasson [8] investigated the non-uniform potential operation in networked-SOFC stacks combined with a gas turbine cycle. They concluded that an increase in the electrical efficiency of 5% could be achieved by improving the thermal management. Also, Au et al. [9] found that 0.6% improvement in the electrical efficiency could be achieved for molten carbonate fuel cell (MCFC) when the concept of non-uniform potential operation was applied [9]. The implementation of this concept in polymer electrolyte membrane fuel cell (PEMFC) was also examined [10]. The results indicated that PEMFC implementing the concept of non-uniform potential operation offered 6.5% improvement in the power density compared with the conventional PEMFC. Vivanpatarakij et al. [11] investigated the implementation of this concept by considering power density as a performance indicator and achieved 9.2% enhancement in the power density by implementing a non-uniform potential operation. Although, non-uniform potential operation improved the performance of SOFC, further operating parameters such as the thermal behavior of solid part inside SOFC stack implementing this concept would promote even more the performance as a large amount of heat is generated due to the irreversibility of the electrochemical mechanism at higher level of the electrical generation. Recently, Guan et al. [12] developed an experimental method to measure temperatures inside stacks using thin K-type thermocouples and self-developed CAS-I sealing materials. The results have shown that temperature distribution of unit cells was non-uniform: the maximum temperature difference between inlet and outlet was about 200 K. The lack of knowledge in the selection of the operating conditions would cause high temperature gradients along the SOFC stack and some solid parts in the stack would be damaged.

In this study, the implementation of "non-uniform potential operation" concept in SOFC fueled by pre-reformed methane was examined using one-dimensional analysis (1-D analysis) for the investigation of stack performance and thermal behavior along the SOFC stack. The calculation using 1-D analysis could well represent the actual SOFC stack behavior as reported by Sorrentino et al. [13]. Methane is an attractive fuel gas as it is present at high concentrations in several fossil and renewable sources such as natural gas [14,15] and biogas [16]. The utilization of methane as a fuel in SOFC has been widely studied [17–20]. Methane could be directly used as a fuel in an anode chamber of SOFC stack; the performance of methane-fueled SOFC stack was significantly lower than that of H_2-fueled SOFC stack as described in our recent work [21]. Moreover, direct utilization of methane in SOFC stack caused inhibition of the performance of SOFC stack due to carbon-deposited blocking inside anode pore [22]. Therefore, the pre-reformer is preferable to be installed in SOFC system in order to initially convert methane into hydrogen. An installation of pre-reformer not only inhibits carbon blockage in the anode chamber but also enhances the power density of the SOFC stack [23]. In this study, the average stack power density is considered as a performance indicator. Operating parameters and SOFC stack configuration are varied to examine operation patterns, inlet temperature and operating voltage that offer maximum power density under stringent thermal constraints i.e. maximum acceptable stack temperature gradient ($T_{G,acp}$) and maximum acceptable stack temperature ($T_{max,acp}$). Moreover, a new configuration of installing inter-cooler with non-uniform potential SOFC operation is proposed to achieve higher average power density.

2. Modeling

The operation of SOFC takes place at the following configuration. The reformed methane is fed into the SOFC stack at the entrance of anode chamber, while air, performing as the oxidizing agent, is fed at the entrance of cathode chamber of SOFC stack. Anode and cathode chambers are separated from each other by solid electrolyte. Inside the cathode, oxygen present in air is reduced to oxygen ions (Eq. (1)) which permeate via the solid electrolyte to the anode chamber where the reaction between oxygen ions and hydrogen takes place to generate steam (Eq. (2)). CO electro-oxidation was assumed to be negligible due to its lower reaction rate compared with H_2 electro-oxidation [24], and to be consumed in the anode chamber via water–gas-shift (WGS) reaction, where reaction rates are high at elevated operating temperatures [25–27]. The SOFC is composed of an anode chamber (Ni–yttria stabilized zirconia), an electrolyte (yttria stabilized zirconia), and a cathode chamber (Lanthanum strontium manganite–yttria stabilized zirconia).

$$\frac{1}{2}O_2 + 2e^- \rightarrow O^{2-} \tag{1}$$

$$H_2 + O^{2-} \rightarrow H_2O \tag{2}$$

The open circuit voltage (E^j) was calculated using the Nernst equation (Eq. (3)).

$$E^j = E_0^j + \frac{RT_e^j}{2F} \ln\left(\frac{p_{H_2}^j \left(p_{O_2}^j\right)^{1/2}}{p_{H_2O}^j}\right) \tag{3}$$

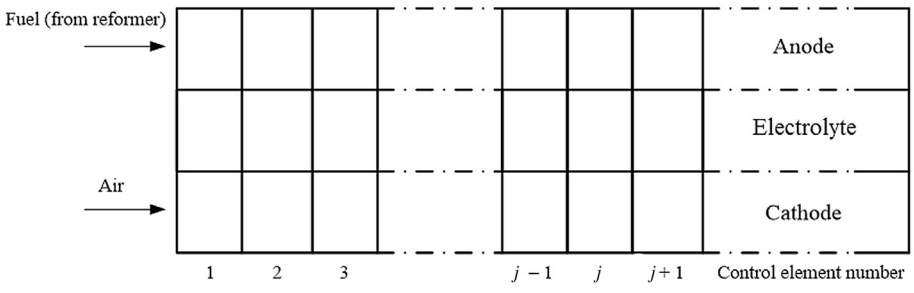

Fig. 1. A small element divided for the calculation in SOFC cell.

Irreversible loss generated inside the SOFC stack was calculated in term of overpotential. The difference between open circuit voltage and the summation of all irreversible loss was named operating voltage (Eq. (4)). In this study, three major types of overpotential were taken into account: activation overpotential, ohmic overpotential and concentration overpotential. The estimation of these overpotentials was given in our recent work [28].

$$V = E^j - \eta^j_{act} - \eta^j_{ohm} - \eta^j_{con} \tag{4}$$

Inside the anode chamber, H_2 was consumed via the electrochemical reaction. Additional hydrogen is obtained via methane steam reforming (Eq. (5)) and WGS (Eq. (6)). The rate of methane steam reforming reaction was computed using Eq. (7) [29], while WGS was assumed at chemical equilibrium due to its fast reaction rates at high operating temperatures [25–27]. Equations of mass and energy balances were solved for each small controlled volume (1-mm distance) (Fig. 1) via one-dimensional (1-D) finite difference method in the flow direction of SOFC stack using computer coding in Visual Basic for MS Excel. The following assumptions were applied in order to simplify the calculation: (i) SOFC stack was operated in adiabatic mode; (ii) heat radiation between solid components inside the stack was neglected [13]; (iii) heat conduction in the solid electrolyte was neglected [13]; (iv) only electrochemical reaction via H_2 electro oxidation takes place; (v) pressure drop generation due to the flow of gas along the stack was neglected. The calculation of mass balance around the control volume was performed using Eqs. (8) and (9) for the anode and cathode chambers, respectively.

$$CH_4 + H_2O \leftrightarrow CO + 3H_2 \tag{5}$$

$$CO + H_2O \leftrightarrow H_2 + CO_2 \tag{6}$$

$$r^j_{ref} = 4274A^j e^{-\left(\frac{82000}{RT^j_a}\right)} p^j_{CH_4}\left(1 - \frac{p^j_{CO}\left(p^j_{H_2}\right)^3}{p^j_{CH_4}p^j_{H_2O}K^j_{ref}}\right) \tag{7}$$

$$N^{j+1}_{a,k} = N^j_{a,k} + \sum_n \nu_{k,n} r^j_n + \frac{\nu_{k,elec} i^j A^j}{2F} \tag{8}$$

$$N^{j+1}_{c,k} = N^j_{c,k} + \frac{\nu_{k,elec} i^j A^j}{2F} \tag{9}$$

Operating voltage was assumed to be constant along the SOFC stack as its current collector usually has a high electrical conductivity. Heat generation in electrolyte due to the irreversibility of electrochemical mechanism and exothermic WGS are transferred into the bulk gas flow inside anode and cathode chambers through heat convection phenomena. Energy balance around solid tri-layer for each control volume was performed using Eq. (10). The energy balance of bulk fluid flow for anode and cathode chambers was calculated via Eqs. (11) and (12), respectively.

$$H^{j+1}_a = H^j_a + h_a A^j\left(T^j_e - T^j_a\right) \tag{11}$$

$$H^{j+1}_c = H^j_c + h_c A^j\left(T^j_e - T^j_c\right) \tag{12}$$

$$-h_a A^j\left(T^j_e - T^j_a\right) - h_c A^j\left(T^j_e - T^j_c\right) + \left[\frac{(-\Delta H)^j_{elec}}{2F} - V\right] i^j A^j + \sum_n r^j_n (-\Delta H)^j_n = 0 \tag{10}$$

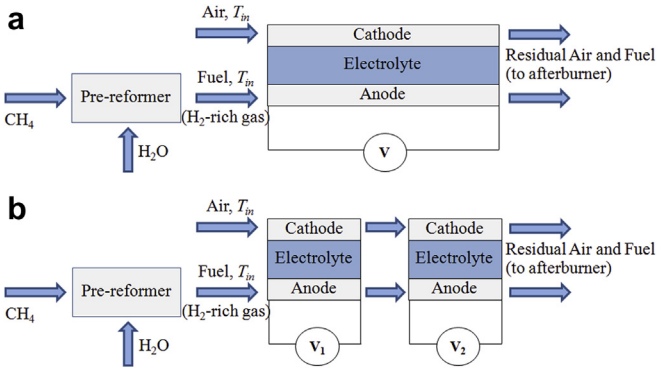

Fig. 2. Material flow schemes of a) uniform potential SOFC stack (1-section SOFC), and b) non-uniform potential SOFC with two sections (2-section SOFC).

To evaluate the viability of SOFC stack, two parameters were considered: the maximum stack temperature gradient (T_G) and the maximum stack temperature (T_{max}). The former parameter was defined as maximum spatial temperature change in electrolyte along the stack length and the maximum stack temperature was designated as maximum value of temperature along the SOFC stack. The maximum acceptable stack temperature gradient ($T_{G,acp}$) of 10 K cm^{-1} [30] and maximum acceptable stack temperature ($T_{max,acp}$) of 1273 K were set as thermal constraints for the viable operation of SOFC stack in this study. The technical terms, i.e. average current density (i_{avg}), average power density (p_{avg}), total fuel utilization (U_f), electrical efficiency (η) and %excess air (ε_{air}) were defined as expressed below;

$$i_{avg} = \frac{\sum_j i^j A^j}{\sum_j A^j} \tag{13}$$

$$p_{avg} = i_{avg} V \tag{14}$$

$$U_f = \frac{\left(\frac{\sum_j i^j A^j}{2F}\right)}{4F_{CH_4}} \tag{15}$$

$$\eta = \left[\frac{P}{\left(LHV_{fuel,in}\right)\left(F_{fuel,in}\right)}\right] \times 100 \tag{16}$$

$$\varepsilon_{air} = \left[\frac{0.21\left(F_{air,in}\right)}{2F_{CH_4}}\right] \times 100 \tag{17}$$

Methane was assumed to be initially reformed using steam to methane molar feed ratio of 2.5 operated at SOFC feed temperature (T_{in}) prior to be fed to the anode chamber of SOFC stack as shown in Fig. 2. Chemical equilibrium was assumed for this reforming reaction in the pre-reformer. The term “methane flow rate, F_{CH_4}” represents methane feed rate to the reformer and the term “% excess

Table 1
Summary of model parameters used in 1-D analysis [33–34].

Parameters	Value
SOFC cell	
l_a	750 μm
l_c	50 μm
L	50 μm
Cell length	400 mm
Cell width	100 mm
Anode channel height	1 mm
Cathode channel height	1 mm
$h_a = h_c$	0.2 kJ m^{-2} s^{-1} K^{-1}
Operating pressure	1 bar

air, ε_{air}" was defined as percent of oxygen feed rate (to cathode chamber) to the stoichiometric flow rate of air for complete combustion of F_{CH_4}. The values of ε_{air} and F_{CH_4} were kept constant at 240% and 1.08 mol h^{-1}, respectively.

3. Results and discussion

The SOFC stack dimensions and input parameters were initially set as summarized in Table 1. Model verification for the calculation of SOFC stack's performance was performed as described in our previous work [31]. The verifying results confirmed that the utilized SOFC stack model could well predict the experimental results of Zhao and Virkar [32] for the mixture of 97% H_2 and 3% CO.

To improve the performance and operating viability of SOFC, the comparison between the performance of 1-section SOFC (Fig. 2a) and 2-section SOFC (Fig. 2b) was first investigated. Inlet temperature of reformed methane and air was set at 998 K, while the operating voltage of SOFC stack was varied until its optimum value which offers the highest average power density was obtained. As shown in Fig. 3a and b, with the optimum operating voltage of 0.778 V, maximum power density was found at the stack length of 0.25 m while stack temperature and temperature gradient were always lower than their maximum acceptable values along the SOFC stack. Concentration of hydrogen in anode gas continuously decreased in the flow direction (Fig. 3b) due to the utilization of hydrogen in the electrochemical reaction. In the first half of SOFC stack, the power density increased in the flow direction until its maximum value was reached due to the decrease in overpotential (increase in stack temperature). However, near the gas exit of the stack, the power density decreased along the flow direction. This was due to both the decrease in hydrogen concentration (Fig. 3b) and rate of electrochemical reaction. Moreover, the open circuit voltage became very low near the gas exit (Fig. 3c) due to the high stack temperature. This would imply that the effect of the decrease in hydrogen concentration in anode bulk gas and open circuit voltage dominated the effect of the decrease in overpotential near the gas exit of SOFC stack. From the calculations, for the case of 1-section SOFC, the optimum operating voltage of 0.778 V could provide average power density and fuel utilization of 0.29 W cm^{-2} and 0.645, respectively.

From the results observed with the 1-section SOFC, the difference between the open circuit voltage and operating voltage is very high and becomes lower at the exit point of the stack (Fig. 3c). This envisions different behaviors inside the SOFC stack and suggests that division of SOFC stack into various sections with different operating voltage may improve the average power density of SOFC stack. The performance of 2-section SOFC was therefore considered using two scenarios: (a) 2-section SOFC with high voltage at the 1st

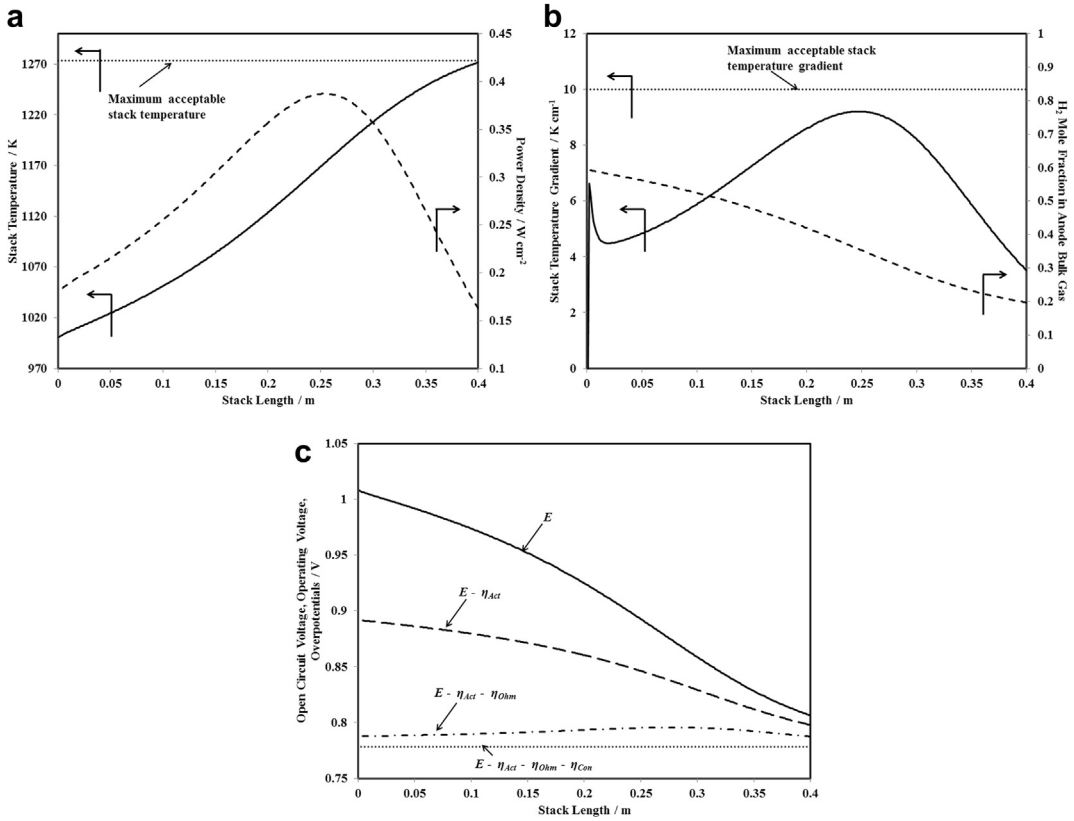

Fig. 3. The distributions of a) stack temperature and power density, b) stack temperature gradient and H_2 concentration in anode bulk gas, and c) open circuit voltage/operating voltage/overpotential along the stack for 1-section SOFC at maximum average power density (T_{in} = 998 K with optimal operating voltage of 0.778 V).

section (2S–1 V) and (b) 2-section SOFC with high voltage at the 2nd section (2S–2 V). For the section operating at high operating voltage, the operating voltage and the low-voltage section were set to 0.8 V and 0.76 V, respectively. To evaluate the stack performance for these scenarios, the 1-section SOFC operating at the optimum operating voltage was considered as a base case. The performance of the 2-section SOFC illustrated in terms of power density, operating voltage and fuel utilization is demonstrated in Figs. 4 and 5. For 2S–1 V scenario (Fig. 4), the power density at the 1st section is lower than the base case although the operating voltage was higher than that of the base case. This is because the increase in temperature and also fuel utilization were lower, and the power density was therefore inhibited. However, 2S–1 V offered a higher power density at the 2nd stack section compared with the base case. This could be explained by the fact that there were large amounts of remaining H_2 fed to the 2nd section of anode chamber due to low fuel utilization in the 1st section of stack, leading to high electrochemical reaction rate at the 2nd section of SOFC stack and hence a higher power density. Due to high fuel utilization at the 2nd section of stack, the increase in stack temperature of 2S–1 V was also higher when compared with that of the base case. For 2S–2 V scenario (Fig. 5), superior power density to the base case was

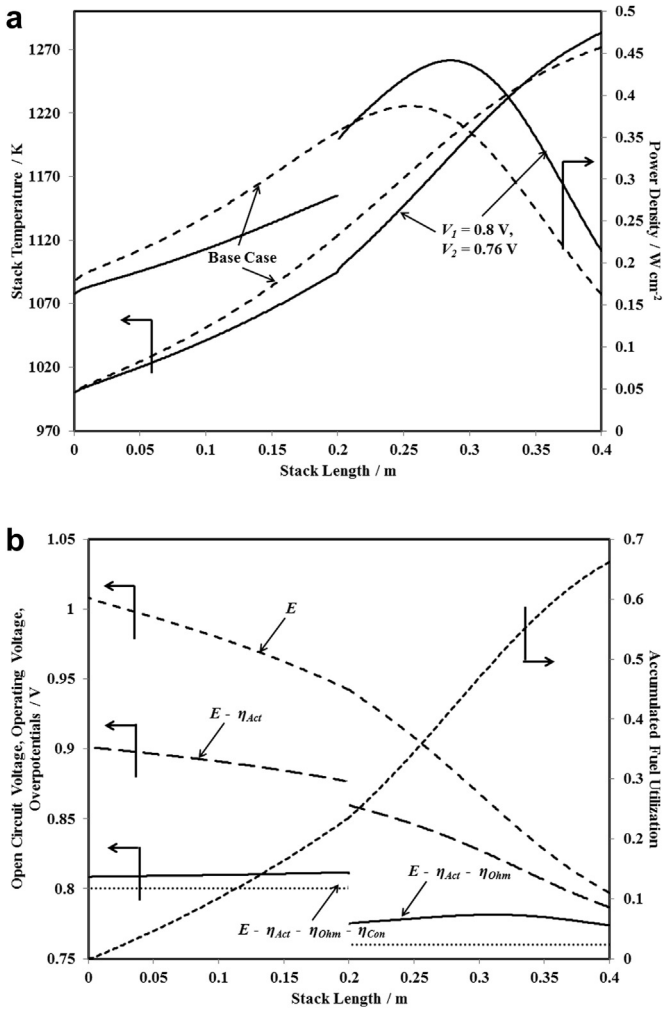

Fig. 4. The distribution of a) power density and stack temperature and b) open circuit voltage/operating voltage/overpotential and accumulated fuel utilization along the stack between the base case and 2-section SOFC with $V_1 = 0.8$ V and $V_2 = 0.76$ V ($T_{in} = 998$ K).

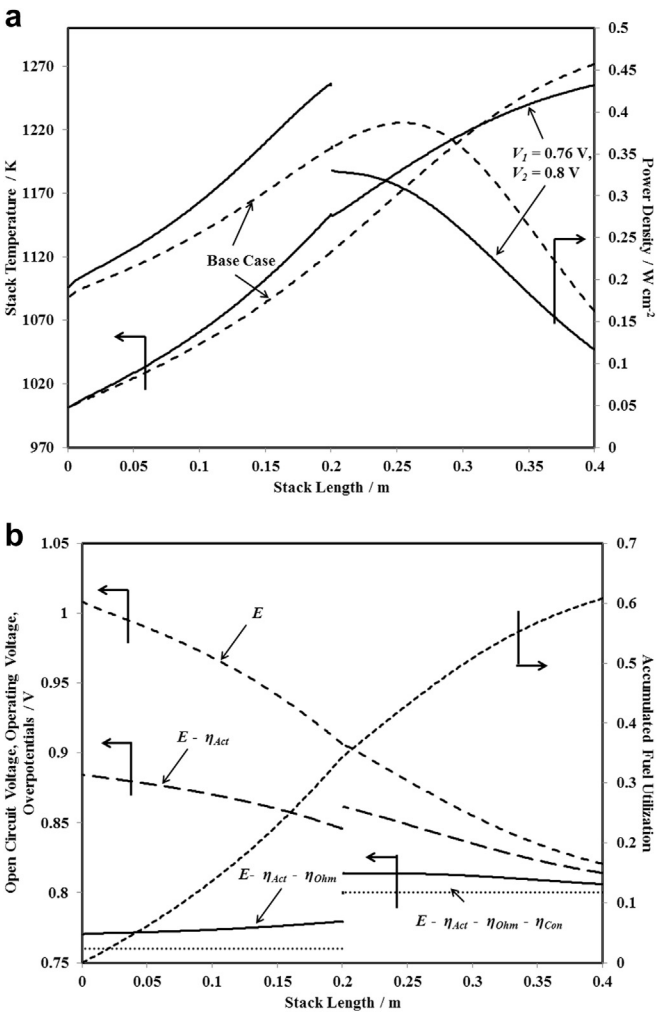

Fig. 5. The distribution of a) power density and stack temperature and b) open circuit voltage/operating voltage/overpotential and accumulated fuel utilization along the stack between the base case and 2-section SOFC with $V_1 = 0.76$ V and $V_2 = 0.8$ V ($T_{in} = 998$ K).

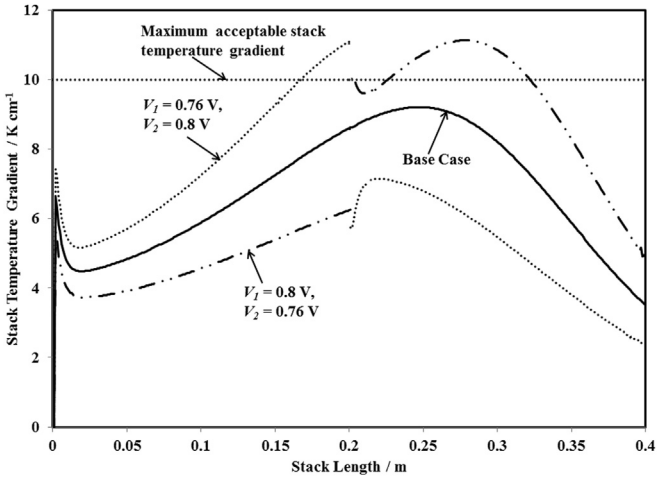

Fig. 6. Comparison of the distribution of stack temperature gradient along the stack between the base case, 2-section SOFC with $V_1 = 0.76$ V and $V_2 = 0.8$ V, and 2-section SOFC with $V_1 = 0.8$ V and $V_2 = 0.76$ V ($T_{in} = 998$ K).

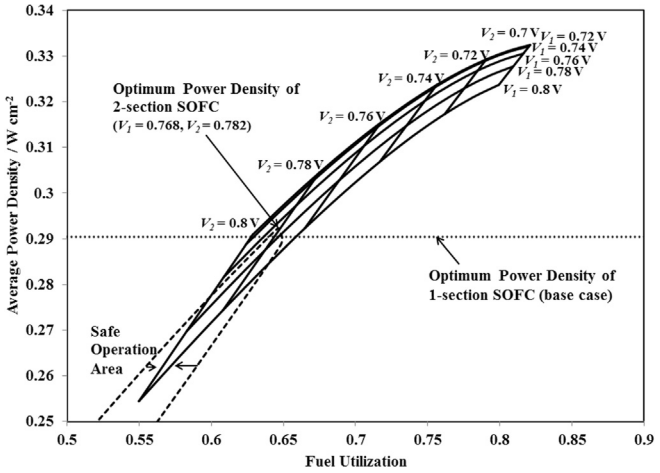

Fig. 7. Effect of operating voltage (V_1 and V_2) on the average power density and fuel utilization of 2-section SOFC (T_{in} = 998 K).

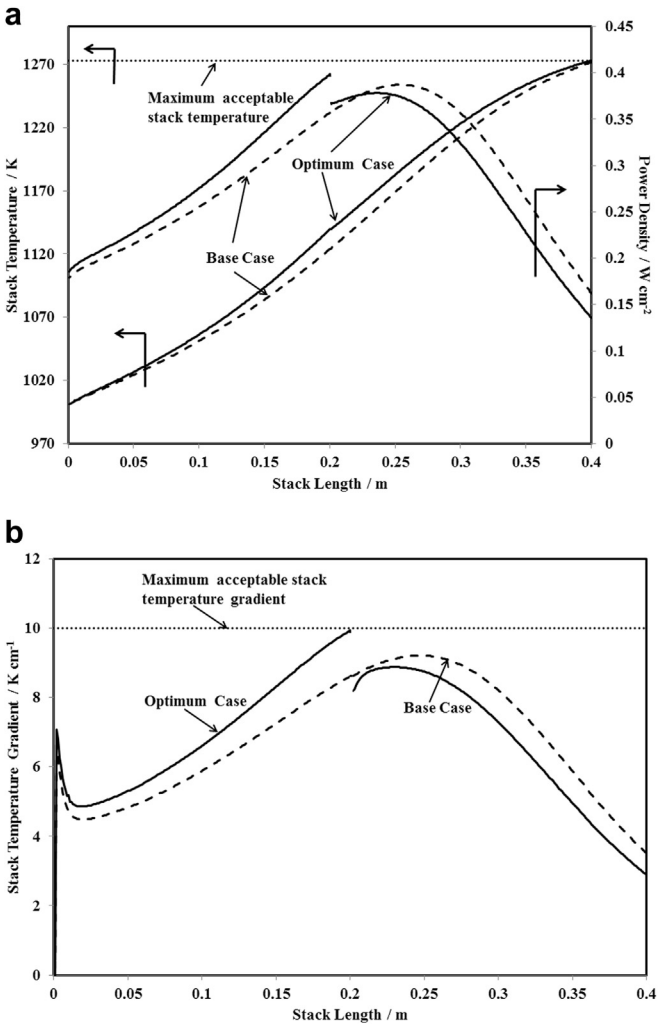

Fig. 8. The distribution of a) stack temperature and power density and b) stack temperature gradient along the stack between the base case and the optimum operation of 2-section SOFC (T_{in} = 998 K).

achieved at the 1st stack section due to higher fuel utilization. This also caused a sharp increase of temperature in the 1st stack section for 2S–2 V. However, the power density of 2S–2 V in the 2nd stack section became lower when compared with that of the base case. This might be due to lower H_2 concentration and rate of electrochemical reaction. These results imply that the difference in the open circuit voltage and operating voltage majorly controlled the fuel utilization as shown in Fig. 5b, the voltage difference increased along with the fuel utilization rate. The accumulated fuel utilization presented in Figs. 4b and 5b for 2S–1 V and 2S–2 V, respectively, indicates the total fuel utilization from the gas entry of SOFC stack to the specified stack position. An increase in the voltage difference represents a high overpotential making the temperature gradient at the 1st stack section for 2S–2 V and at the 2nd stack section for 2S–1 V over the limit as shown in Fig. 6. It could be concluded that the decrease in operating voltage enhances the power density; however, thermal constraint of SOFC operation could also be infringed. By considering the reason above, the selection of suitable operating voltage for 2-section stack should be carefully considered.

The values of operating voltage for the 1st section (V_1) and 2nd section (V_2) of 2-section SOFC stack were varied to study their effects on average power density and fuel utilization as shown in Fig. 7. The results demonstrate that the decrease in V_1 and V_2 could improve the average power density and also promote fuel utilization of SOFC stack. However, it is not likely that operation of 2-section SOFC offered a greater average power density than the base case under the safe operation area (the area where the operating conditions offered T_G and T_{max} below their maximum acceptable values). In this work, the optimum values of V_1 and V_2 of 2-section SOFC were found to be at 0.768 and 0.782 V, respectively (Fig. 7). As summarized in Table 2, an insignificant improvement of 0.69% in average power density of 2-section SOFC over 1-section SOFC is observed. At the optimum

Table 2
Comparison of the performance of the optimum cases of 1-section SOFC, 2-section SOFC, 2-section SOFC-T and 3-section SOFC-T.

Operation mode	Optimum case of 1-section SOFC	Optimum case of 2-section SOFC	Optimum case of 2-section SOFC-T	Optimum case of 3-section SOFC-T
$F_{CH_4,eq}$ (mol s^{-1})	0.0003	0.0003	0.0003	0.0003
ε_{air} (%)	240	240	240	240
U_f (–)	0.6451	0.6462	0.7739	0.7425
Operating voltage (V)	0.778	V_1 = 0.768 V_2 = 0.782	V_1 = 0.79 V_2 = 0.731	V_1 = 0.789 V_2 = 0.755 V_2 = 0.719
Average Power density (W cm^{-2})	0.2903	0.2923	0.3274	0.3090
Average Current density (A cm^{-2})	0.3732	0.3738	0.4479	0.4297
η (%)	39.13	39.40	44.13	41.65
Electricity produced (W)	116.14	116.93	130.96	123.60
Maximum stack temperature (K)	1271.71	1273.11	1227.57	1169.14
Maximum stack temperature gradient (K cm^{-1})	9.21	9.93	9.94	9.97

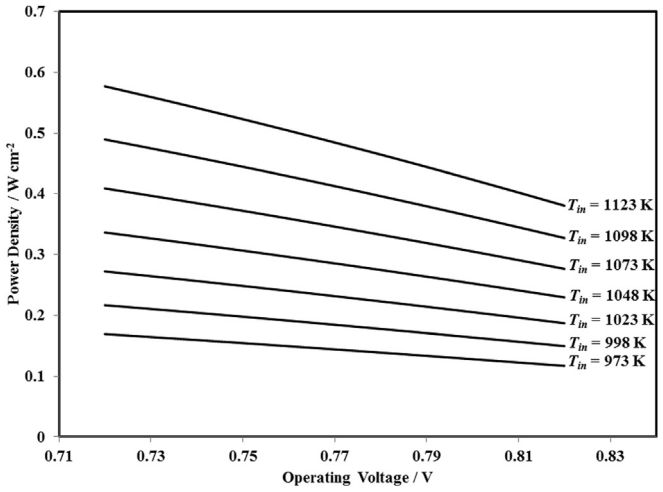

Fig. 9. Effect of operating voltage and operating temperature on power density of SOFC calculated based on the chemical equilibrium composition of steam methane reforming reaction with the steam to carbon ratio of 2.5.

operation, the profiles of power density, stack temperature, and stack temperature gradient along the SOFC stack of 2-section SOFC were almost similar to those of the base case as shown in Fig. 8a and b. This is due to the narrow thermal-safe operation area which limited the operation of 2-section SOFC (Fig. 7). It could be concluded that the operation of 2-section SOFC with the consideration of a solely operating voltage cannot significantly improve the SOFC performance.

As discussed previously, although the stack temperature played the major role in controlling the stack performance, thermal constraint is another important factor that could limit its performance. In Fig. 9, it is shown the effect of operating voltage and operating temperature on the power density of SOFC operation, which were calculated based on the chemical equilibrium composition of methane steam reforming reaction. The results show that the power density was improved when SOFC was operated at high temperature and low operating voltage. To further envision the effect of stack temperature on the SOFC performance, the effect of inlet temperature of fuel and air (T_{in}) was studied for 1-section SOFC. The results, as demonstrated in Fig. 10, show that despite the fact that the operation of SOFC at high temperature and low voltage could offer a high power density, this operation was still impractical as T_G and T_{max} exceeded their limiting values. As shown in Fig. 10a and b, when T_{in} was higher than 998 K, the operation of 1-section SOFC was controlled by the constraint of $T_{max,acp}$, while the constraint of $T_{G,acp}$ became an operation-controlling criteria as the inlet fuel temperature was lower than 998 K. Moreover, for high T_{in}, 1-section SOFC could not be operated at low operating voltage due to the thermal constraints. To overcome the thermal constraints, values of the operating voltage larger than 0.81 V were required when T_{in} is 1048 K, while a value of the operating voltage as low as 0.778 V could be operated for 1-section SOFC operating at T_{in} of 998 K (Fig. 10a). Operation of SOFC at a higher T_{in} (ranging from 1048 K to 998 K) caused lower average power density (Fig. 10a) and total fuel utilization (Fig. 10c).

To operate at favored conditions (high temperature and low operating voltage) with the thermal-secured operation, the new SOFC configuration, "non-uniform potential and 2-section SOFC

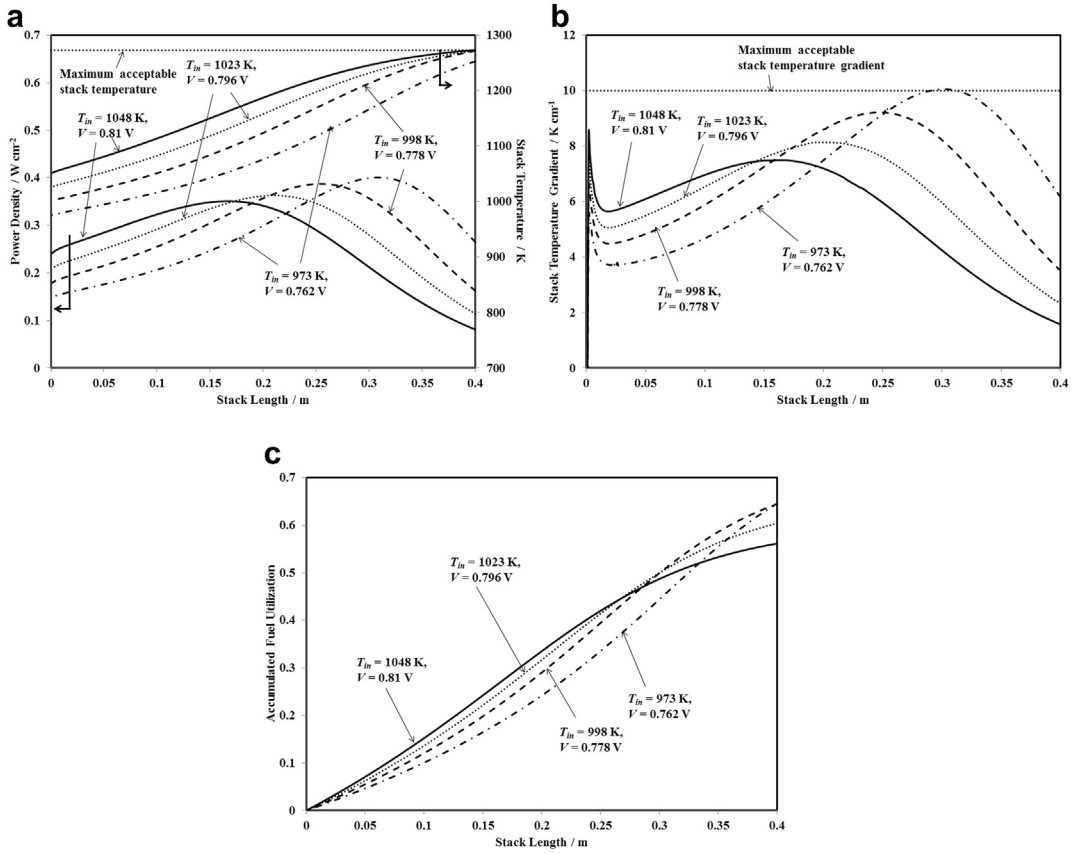

Fig. 10. The distribution of a) stack temperature and power density, b) stack temperature gradient, and c) accumulated fuel utilization along the SOFC stack for the optimum operation of 1-section SOFC at different T_{in}.

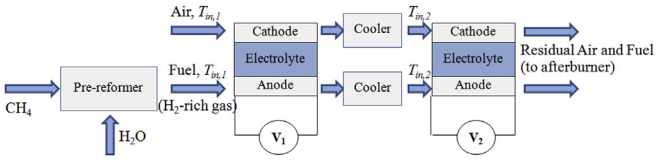

Fig. 11. Schematic diagram of non-uniform potential 2-section SOFC stack equipped with cooler, 2-section SOFC-T.

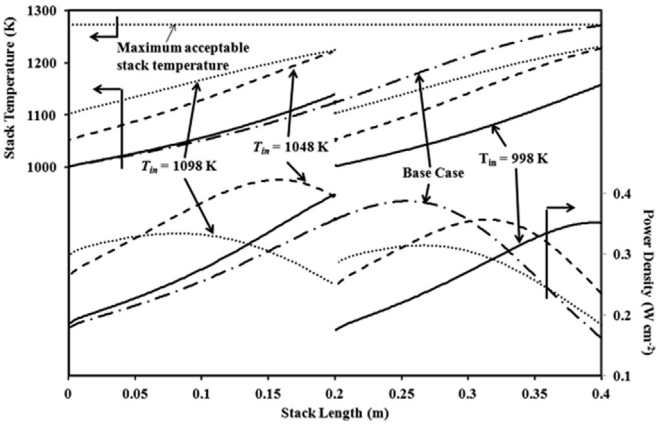

Fig. 12. The distribution of stack temperature and power density along the SOFC stack for the optimum case of 2-section SOFC-T operating at different T_{in}.

stack equipped with a cooler, (2-section SOFC-T)" was proposed. The scheme of this configuration was similar to that of 2-section SOFC, except installation of an additional cooler between the first and the second sections of the stack as shown in Fig. 11. With this configuration, the outlet gas streams from the cathode and anode chambers of the 1st section of stack were fed to the cooler, where temperature of gas stream was reduced to $T_{in,2}$ prior to be fed to the 2nd section of stack. The effects of inlet temperatures ($T_{in,1}$) and ($T_{in,2}$) of fuel and air for the 1st and 2nd stack sections, respectively, as well as those of operating voltages (V_1) and (V_2) of the 1st and the 2nd stack sections, respectively, on performance of 2-section SOFC-T were studied. To simplify the calculations, $T_{in,1}$ was assumed equal to $T_{in,2}$ and both of them were similar to T_{in}.

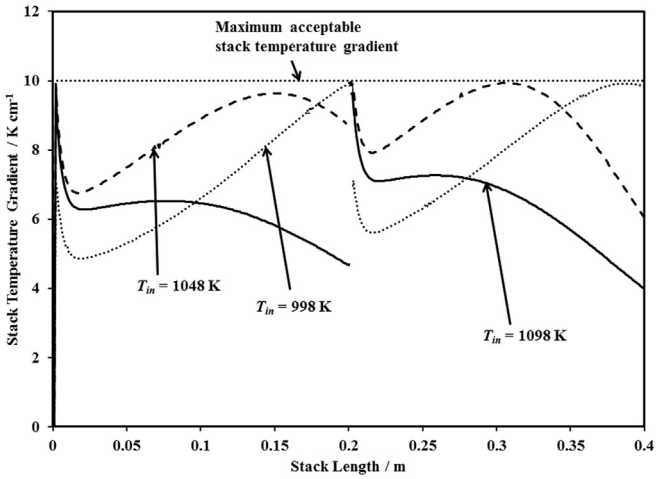

Fig. 13. The distribution of stack temperature gradient along the SOFC stack for the optimum operation of 2-section SOFC-T at different T_{in}.

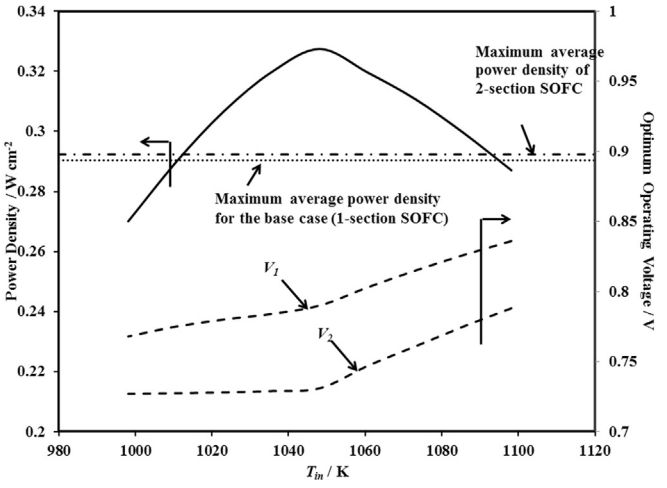

Fig. 14. Power density and optimum V_1, and V_2 of 2-section SOFC-T at different T_{in}.

The operating voltages V_1 and V_2 were varied until their optimum values (the value that allowed the maximum average power density of 2-section SOFC-T) were achieved and all thermal constraints were pursued. The stack temperature and power density profiles for the optimum case of 2-section SOFC-T along the stack with the variation of T_{in} are illustrated in Fig. 12. The results show that T_{max} of 2-section SOFC-T operated at T_{in} between 998 K and 1098 K were largely lower than those of the base case (1-section SOFC) and $T_{max,acp}$. Therefore, the thermal constraint for the operation of 2-section SOFC-T was the controlling of T_G of SOFC stack to be lower than $T_{G,acp}$. As shown in Fig. 13, unlike the 1-section SOFC and 2-section SOFC, the limitation of the value of T_G is challenged with the operation of 2-section SOFC-T, especially for the operation at T_{in} = 1048 K, where this situation is found at both gas entry and middle position of the two SOFC sections. The thermal constraint challenge at the gas entry was caused by the high H_2 concentration of anode fuel gas stream that accelerates the rate of electrochemical reaction at this stack position, while the challenge at the middle of the stack was caused by the enhancement in the electrochemical reaction rate due to the increase in stack temperature. However, the selection of the appropriate T_{in} is also an important issue for the control of the performance of 2-section SOFC-T. At T_{in} = 998 K, the thermal constraint challenge for 2-section SOFC-T is found only at near the gas exit of both two sections. For the case that T_{in} = 1098 K, the thermal constraint was challenged only at the gas entries of each section. This is because the rate of electrochemical reaction at the gas entry was very high due to its high operating temperature. Moreover, with high T_{in}, desirable low operating voltage could not be operated due to the thermal constraint at the gas entry. The summary of average power density and optimum operating voltage at different T_{in} of 2-section SOFC-T are given in Fig. 14. The maximum power density of 0.327 W cm^{-2} was achieved at T_{in} = 1048 K and optimum values of V_1 and V_2 of 0.79 and 0.731 V, respectively. The maximum average power density of 2-section SOFC-T is 12.77% higher than that of the base case (1-section SOFC). If T_{in} was lower than its optimum value, average power density of 2-section SOFC-T became lower due to lower electrochemical reaction rate. Increase in power density of 2-section SOFC-T was also inhibited when operating at high T_{in} (Fig. 14). This is due to the fact that low desirable operating voltage cannot be operated at high T_{in} owing to the thermal constraint. The 2-section SOFC-T could offer a higher stack performance compared with the 1-section SOFC.

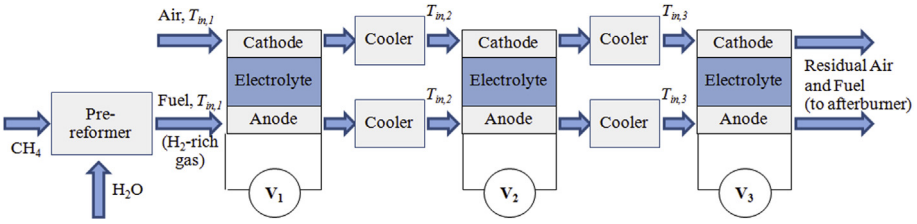

Fig. 15. Schematic diagram of non-uniform potential 3-section SOFC stack equipped with two coolers, 3-section SOFC-T.

To further evaluate the performance of non-uniform potential SOFC stack equipped with a cooler, the non-uniform potential SOFC stack with 3 sections equipped with 2 coolers, 3-section SOFC-T, was proposed as shown in Fig. 15. With this configuration, the length of each stack section was set to be similar to one another while inlet temperatures of fuel gas and air streams for each stack section were assumed similar and equal to T_{in} ($T_{in} = T_{in,1} = T_{in,2} = T_{in,3}$). T_{in} of 3-section SOFC-T was varied and optimum values of V_1, V_2, and V_3 for each T_{in} were examined. As shown in Fig. 16, similar to the case of 2-section SOFC-T, the maximum average power density of 3-section SOFC-T was achieved when $T_{in} = 1048$ K. To achieve the maximum average power density for each T_{in}, V_1 was always set to be higher than V_2 and V_2 to be higher than V_3. It is observed that the increase in the number of sections could not improve the SOFC performance. As summarized in Table 2, maximum achieved average power density of 3-section SOFC-T was 0.309 W cm^{-2}, which was lower than that of 2-section SOFC-T (0.327 W cm^{-2}). As shown in Fig. 17a, since the length of each stack section of 3-section SOFC-T was too short, its power density could not reach its maximum value. With the defined SOFC stack dimension and electrochemical reaction rate, unlike 2-section SOFC-T, adequately high stack temperature could not be achieved at the gas exit of each section for 3-section SOFC-T as shown in Fig. 17b. This result reveals that, apart from the operating voltage, average power density as well strongly depended on the stack temperature.

It is noted that this work presented the success of applying non-uniform potential SOFC with a novel inter-cooler to overcome the limitation of temperature gradient by trial methodology. However, using complete optimization methodology could offer more precise suitable operating parameters. In addition, the effects of other design parameters such as the length of each stack section, the gas inlet temperature for each stack section, and % excess air should also be considered.

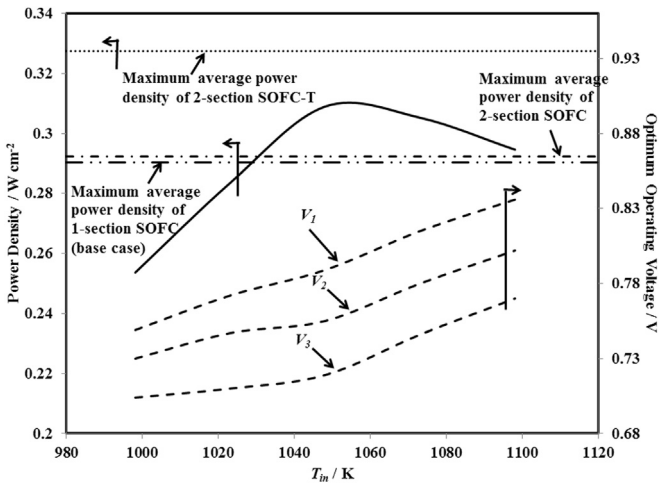

Fig. 16. Power density and optimum V_1, V_2, and V_3 of 3-section SOFC-T at different T_{in}.

4. Conclusion

In this study, one-dimensional finite difference method was applied to evaluate the performance of non-uniform potential SOFC stack. Power density was considered as a performance indicator of the operation of SOFC stack fueled by reformed methane. The evaluation was performed based on two thermal constraints: maximum acceptable stack temperature of 1273 K and maximum acceptable stack temperature gradient of 10 K cm^{-1}. Initially, the first proposed non-uniform potential SOFC with two sections (2-section SOFC) was evaluated. With this configuration, SOFC stack was divided into two sections operating at different operating voltages. The values of

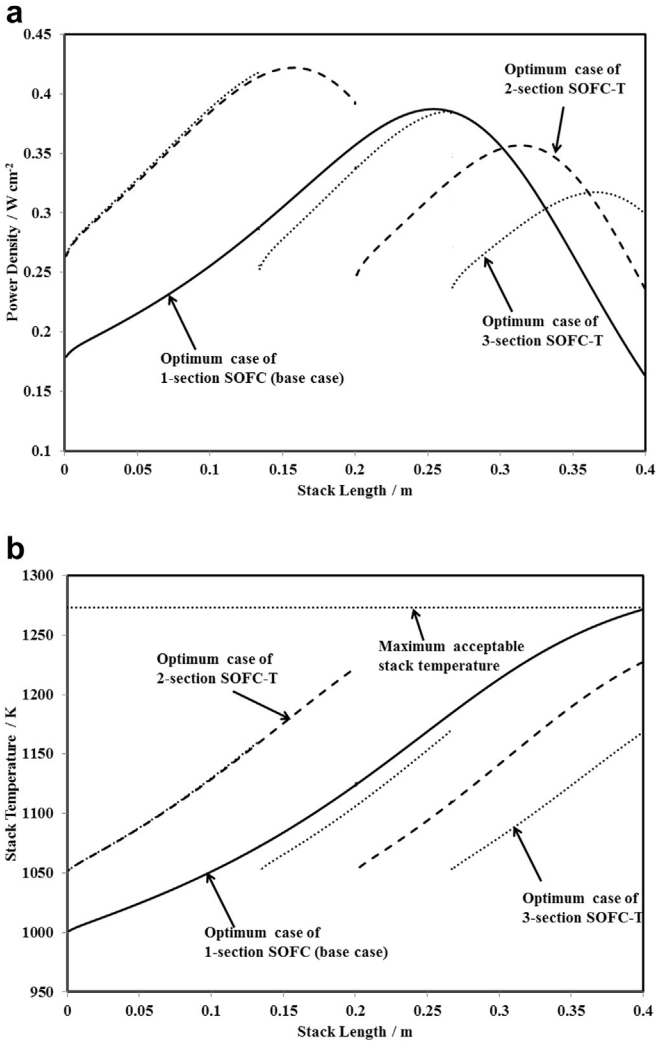

Fig. 17. The distribution of a) power density and b) stack temperature along stack length of the optimum cases of 1-section SOFC, 2-section SOFC-T and 3-section SOFC-T.

operating voltage of each section of 2-section SOFC were varied to determine maximum average power density under the two thermal constraints. The results indicated that 2-section SOFC can offer only 0.69% average power density higher than traditional 1-section SOFC with the optimum values of operating voltage of 0.768 V for the 1st section and of 0.782 V for the 2nd section. To achieve a high power density and simultaneously overcome the thermal constraints, a new configuration of non-uniform potential SOFC, non-uniform potential and 2-section SOFC stack equipped with a cooler (2-section SOFC-T) was proposed. In this configuration, the cooler was installed to reduce temperatures of the fuel gas and air outlet from the 1st section prior to be fed to the 2nd section. It was found that not only operating voltage that played an important role in the operation of 2-section SOFC-T but also the inlet fuel and air temperatures are critical factors affecting the performance of 2-section SOFC-T. The value of the temperature should, therefore, be well selected to overcome the thermal constraints and minimize the overpotential. The maximum average power density of the 2-section SOFC-T was achieved when the inlet fuel temperature was set at 1048 K and the values of operating voltages of the 1st and 2nd sections were equal to 0.79 and 0.731 V, respectively. By operating at this condition, the 2-section SOFC-T offered 12.8% improvement in average power density compared with the 1-section SOFC. With the defined SOFC stack dimension and electrochemical reaction rate, an increase in the number of section from 2 sections to 3 sections (3-section SOFC-T) could not improve the average power density since the high stack temperature was not reached at the gas exit of each section for 3-section SOFC-T and its overpotential was high. Further detailed study should be performed in order to optimize other process parameters of 2-section SOFC-T, such as the length of each stack section and the fuel gas inlet temperature for each stack section.

Acknowledgments

The supports from Postdoctoral fellowship (Ratchadaphisek-somphot Endowment Fund) from Graduate School Chulalongkorn University and the TRF Senior Researcher Scholar from the Thailand Research Fund are gratefully acknowledged.

References

[1] P. Kuchonthara, S. Bhattacharya, A. Tsutsumi, J. Power Sources 124 (2003) 65–75.
[2] M.C. Williams, Fuel Cells 7 (2007) 78–85.
[3] S.P. Yoon, J. Han, S.W. Nam, T.H. Lim, S.A. Hong, J. Power Sources 136 (2004) 30–36.
[4] S.D. Kim, S.H. Hyun, J. Moon, J.H. Kim, R.H. Song, J. Power Sources 139 (2005) 67–72.
[5] Y. Yi, A.D. Rao, J. Brouwer, G.S. Samuelsen, J. Power Sources 132 (2004) 77–85.
[6] V. Liso, Y. Zhao, N. Brandon, M.P. Nielsen, S.K. Kaer, Int. J. Hydrogen Energy 36 (2011) 13715–13726.
[7] H. Wen, J.C. Ordonez, J.V.C. Vargas, Appl. Therm. Eng. 50 (2013) 12–25.
[8] A. Selimovic, J. Palsson, J. Power Sources 106 (2002) 76–82.
[9] S.F. Au, N. Woudstra, K. Hemmes, J. Power Sources 122 (2003) 28–36.
[10] S.M. Senn, D. Poulikakos, Electrochem. Commun. 7 (2005) 773–780.
[11] S. Vivanpatarakij, S. Assabumrungrat, N. Laosiripojana, J. Power Sources 167 (2007) 139–144.
[12] W.B. Guan, H.J. Zhai, L. Jin, C. Xu, W.G. Wang, Fuel Cells 12 (2012) 24–31.
[13] M. Sorrentino, C. Pianese, Y.G. Guezennec, J. Power Sources 180 (2008) 380–392.
[14] G. Karavalakis, T.D. Durbin, M. Villela, J.W. Miller, J. Nat. Gas Sci. Eng. 4 (2012) 8–16.
[15] G.P. McTaggart-Cowan, S.N. Rogak, S.R. Munshi, P.G. Hill, W.K. Bushe, Fuel 89 (2010) 752–759.
[16] R.J. Spiegel, J.L. Preston, J. Power Sources 86 (2000) 283–288.
[17] Y. Patcharavorachot, A. Arpornwichanop, in: Proceedings of the 22nd European Symposium on Computer Aided Process Engineering, 17–20 June 2012. London.
[18] K. Nikooyeh, A.A. Jeje, J.M. Hill, J. Power Sources 171 (2007) 601–609.
[19] E. Vakouftsi, G. Marnellos, C. Athanasiou, F.A. Coutelieris, Chem. Eng. Res. Des. 89 (2011) 224–229.
[20] Y. Wang, F. Yoshiba, M. Kawase, T. Watanabe, Int. J. Hydrogen Energy 34 (2009) 3885–3893.
[21] P. Piroonlerkgul, W. Wiyaratn, A. Soottitantawat, W. Kiatkittipong, A. Arpornwichanop, N. Laosiripojanad, S. Assabumrungrat, Chem. Eng. J. 155 (2009) 411–418.
[22] S. Baron, N. Brandon, A. Atkinson, B. Steele, R. Rudkin, J. Power Sources 126 (2004) 58–66.
[23] V.M. Janardhanan, V. Heuveline, O. Deutschmann, J. Power Sources 172 (2007) 296–307.
[24] M.A. Khaleel, Z. Lin, P. Singh, W. Surdoval, D. Collin, J. Power Sources 130 (2004) 136–148.
[25] R. Blom, I.M. Dahl, A. Slagtem, B. Sortland, A. Spjelkavik, E. Tangstad, Catal. Today 21 (1994) 535–543.
[26] M.C.J. Bradford, M.A. Vannice, Appl. Catal. A Gen. 142 (1996) 97–122.
[27] H.M. Swaan, V.C.H. Kroll, G.A. Martin, C. Mirodatos, Catal. Today 21 (1994) 571–578.
[28] P. Piroonlerkgul, S. Assabumrungrat, N. Laosiripojana, A.A. Adesina, Chem. Eng. Process. Process Intensif. 48 (2009) 672–682.
[29] E. Achenbach, E. Riensche, J. Power Sources 52 (1994) 283–288.
[30] L.T. Lim, D. Chadwick, L. Kershenbaum, Ind. Eng. Chem. Res. 44 (2005) 9609–9618.
[31] P. Piroonlerkgul, S. Assabumrungrat, N. Laosiripojana, A.A. Adesina, Chem. Eng. J. 140 (2008) 341–351.
[32] F. Zhao, A.V. Virkar, J. Power Sources 141 (2005) 79–95.
[33] P. Aguiar, D. Chadwick, L. Kershenbaum, Chem. Eng. Sci. 59 (2004) 87–97.
[34] M. Ni, M.K.H. Leung, D.Y.C. Leung, Energy Convers. Manage. 48 (2007) 1525–1535.

Nomenclature

A: SOFC stack active area [m^2]
E: electromotive force [V]
E_0: electromotive force at standard pressure [V]
F: Faraday constant (9.6495×10^4) [C mol^{-1}]
$F_{air,in}$: inlet air flow rate to SOFC [mol s^{-1}]
$F_{CH_4,eq}$: methane equivalent flow rate [mol s^{-1}]
$F_{fuel,in}$: inlet fuel flow rate to SOFC [mol s^{-1}]
h: heat transfer coefficient [W m^{-2} K^{-1}]
ΔH_i: heat of reaction for reaction i [J mol^{-1}]
H: energy rate [J s^{-1}]
i: current density [A cm^{-2}]
K_{ref}: equilibrium constant for steam reforming reaction [Pa^2]
l: thickness [μm]
$LHV_{fuel,in}$: lower heating value of SOFC inlet fuel [J mol^{-1}]
N_k: molar flow rate of component k [mol s^{-1}]
p_k: partial pressure of component k [Pa]
p: power density [W cm^{-2}]
P: electricity produced [W]
r_n: reaction rate for reaction n [mol s^{-1}]
R: gas constant (8.3145) [J mol^{-1} K^{-1}]
T: temperature [K]
T_G: maximum stack temperature gradient [K cm^{-1}]
$T_{G,acp}$: maximum acceptable stack temperature gradient [K cm^{-1}]
T_{in}: SOFC inlet temperature of fuel and air streams [K]
T_{max}: maximum stack temperature [K]
$T_{max,acp}$: maximum acceptable stack temperature [K]
U_f: total fuel utilization [−]
V: operating voltage [V]
V_n: operating voltage of section n [V]

Greek letters
ε_{air}: % excess air [%]
η: electrical efficiency [%]
η_{act}: activation loss [V]
η_{con}: concentration loss [V]
η_{ohm}: ohmic loss [V]
$v_{k,i}$: stoichiometric coefficient of component k in reaction i [−]

Superscript
j: j^{th} control volume (0, 1, 2,…, 400)

Subscripts
a: anode chamber
avg: average
c: cathode chamber
e: electrolyte
$elec$: electrochemical reaction
k: component (CH_4, CO, CO_2, H_2, H_2O, O_2, N_2)
n: reaction (ref, WGS, elec)
ref: reforming reaction
WGS: water gas shift reaction